Composite Structures 271 (2021) 114157

Contents lists available at ScienceDirect

Composite Structures

journal homepage: www.elsevier.com/locate/compstruct

Influences of material gradient and nonlinearity on the forced vibration of orthotropic shell structures

A.H. Sofiyev [a,*], F. Turan [b], N. Kuruoglu [c]

[a] Department of Civil Engineering of Engineering Faculty, Suleyman Demirel University, 32260 Isparta, Turkey
[b] Department of Civil Engineering of Engineering Faculty, Ondokuz Mayıs University, 55139 Samsun, Turkey
[c] Department of Civil Engineering of Faculty of Engineering and Architecture, Istanbul Gelisim University, 34310 Istanbul, Turkey

ARTICLE INFO

Keywords:
Forced vibration
Nonlinearity
Inhomogeneity
Orthotropy
Spherical and hypar shells
Multi-scales method
External excitation

ABSTRACT

In this study, the influences of material gradient and nonlinearity on the forced vibration of orthotropic shell structures under external excitations are investigated for first time. The mathematical model of inhomogeneous orthotropic double-curved shallow shells is built using the Hamilton principle and von Karman-type nonlinearity. The basic equations are reduced to nonlinear ordinary differential equations using the Galerkin procedure. Using the multiscale method, the frequency-amplitude relations of double-curved shallow shells and the nonlinear frequency response of forced vibrations are obtained for first time. The reliability of the obtained expressions is checked by comparison with the literature data. In numerical analysis, the influence of inhomogeneity, orthotropy, nonlinearity, and the external excitation parameter on the frequency of forced vibrations is investigated in detail by performing unique numerical calculations taking into account various profiles of inhomogeneous orthotropic shallow spherical and hyperbolic paraboloidal (or hypar) shells.

1. Introduction

The shallow shells with Gaussian curvature are among the most widely used as structural elements in engineering applications in recent years. One of the most important features of such structural elements is the unique architectural design and the possibility of bridging large openings in two directions without intermediate supports. It is known that shallow shells are subjected to various dynamic loads in their areas of application. One of the most dangerous loads for the reliability and safety of structural elements are periodic dynamic loads that cause forced vibrations [1,2]. The nonlinear effects of forced vibrations of shallow shells create a frequency dependence in the vicinity of the resonant frequency. Unlike natural vibrations, forced vibrations are not damped because they are continuously subjected to external excitation pressures. Since the amplitude of the forced vibrations, as well as the stresses and stresses in the shallow shells, increase significantly, unexpected damage to structural elements may occur. The problem of studying steady-state forced vibrations is applicable to structures used for various purposes, due to the widespread use of loading modes that cause intense resonant vibrations in them. The study of forced vibrations of shells made of homogenous orthotropic materials at finite deflection is critical for the design of aerospace structures, as shown in references [3,4].

The widespread use of shallow shells in modern technologies necessitates the use of the latest materials of the era in their production. One of the material types in this class is inhomogeneous orthotropic composite materials. One of biggest challenges in mathematical modeling of shallow shells composed of inhomogeneous composite materials is the modeling of material heterogeneity. In the literature, the studies on the modeling of properties of inhomogeneous orthotropic materials are limited in number, and solutions are generally produced using these models [5–9]. The most of investigations on the forced vibrations of inhomogeneous shells have been carried out using inhomogeneous isotropic materials. It should be emphasized that these studies are also limited in number [10–20].

In modeling, as the inhomogeneous orthotropic properties of materials forming the shallow shells, as well as the geometric nonlinearity are taken into account, the derivation of fundamental equations and the solution of problem become considerably difficult. For these reasons, there are very few studies on the large amplitude vibration of inhomogeneous orthotropic spherical and hypar shells and these works belong to the solution of free vibration problem [21]. The literature researches show that the nonlinear forced vibration problem of

* Corresponding author.
E-mail addresses: abdullahavey@sdu.edu.tr (A.H. Sofiyev), ferruh.turan@omu.edu.tr (F. Turan), nkuruoglu@gelisim.edu.tr (N. Kuruoglu).

https://doi.org/10.1016/j.compstruct.2021.114157
Received 19 January 2021; Revised 11 April 2021; Accepted 21 May 2021
Available online 24 May 2021
0263-8223/© 2021 Elsevier Ltd. All rights reserved.

spherical and hypar shells made of inhomogeneous orthotropic materials subjected to the external excitation cannot be investigated. The current study is devoted to the solution of this problem.

2. Problem statement

In Fig. 1 shows an inhomogeneous orthotropic a) spherical and (b) hypar shells with the radii of curvature R_1 and R_2 subjected to the time-dependent external excitation $q(t)$. The thickness, length and width of the inhomogeneous orthotropic double-curved shallow shell are h, a_1 and a_2. As usual, the curvilinear orthogonal coordinate system $x_1x_2x_3$ is located at the corner of the inhomogeneous orthotropic double-curved shallow shells on the mid-surface. The displacement components u_1, u_2, u_3 of any point of the inhomogeneous orthotropic double-curved shallow shell are directed to the x_1, x_2, x_3 axes, respectively.

The mechanical properties of inhomogeneous orthotropic double-curved shallow shells are defined by [5–9]:

$$\begin{aligned} &E_{11}^{\bar{x}_3} = Y_{11}^{H} e^{\eta_1(\bar{x}_3+0.5)},\ E_{22}^{\bar{x}_3}(\bar{x}_3) = Y_{22}^{H} e^{\eta_1(\bar{x}_3+0.5)},\\ &E_{12}^{\bar{x}_3} = Y_{12}^{H} e^{\eta_1(\bar{x}_3+0.5)},\ D_{\rho}^{\bar{x}_3} = D_{\rho}^{H} e^{\eta_2(\bar{x}_3+0.5)},\ \bar{x}_3 = x_3/h \end{aligned} \tag{1}$$

where $Y_{ij}^{H}(i,j=1,2)$ denote the elasticity moduli and D_{ρ}^{H} denotes the mass density of homogenous orthotropic materials. Furthermore, $\eta_i(i=1,2)$ depend on the $\bar{x}_3$ coordinate and are the rating coefficients for the elasticity moduli and density, providing the following inequality $-1 \leqslant \eta_i \leqslant 1$ $(i=1,2)$. It is noted that inhomogeneous orthotropic materials turn into homogenous orthotropic materials, at $\eta_i = 0$ $(i=1,2)$.

In Figs. 2 and 3, the variations of elasticity modulus $(E_{11}^{\bar{x}_3})$ of inhomogeneous orthotropic shallow shells consisting of graphite/epoxy in two- and three-dimensional coordinate systems according to the $\bar{x}_3$ coordinate are presented for $\eta_1 = -1$ and $\eta_1 = +1$, respectively. In Figs. 2 and 3, $\bar{x}_1$ is the nondimensional length coordinate and $\bar{x}_1 = x_1/a_1$. The changes of other elastic properties and density depending on the nondimensional thickness coordinate can be drawn similarly.

The plane stress constitutive relations of inhomogeneous orthotropic double-curved shallow shells can be built as follows [21]:

$$\begin{bmatrix}\sigma_{11}\\ \sigma_{22}\\ \sigma_{12}\end{bmatrix} = \begin{bmatrix} q_{11}^{\bar{x}_3} & q_{12}^{\bar{x}_3} & 0\\ q_{21}^{\bar{x}_3} & q_{22}^{\bar{x}_3} & 0\\ 0 & 0 & q_{66}^{\bar{x}_3}\end{bmatrix} \begin{bmatrix} e_{11}^{0} - x_3\frac{\partial^2 u_3}{\partial x_1^2}\\ e_{22}^{0} - x_3\frac{\partial^2 u_3}{\partial x_2^2}\\ e_{12}^{0} - 2x_3\frac{\partial^2 u_3}{\partial x_1 \partial x_2}\end{bmatrix} \tag{2}$$

where $q_{ij}^{\bar{x}_3}(i,j=1,2,6)$ are the transformed reduced stiffness described by,

$$q_{ii}^{\bar{x}_3} = \frac{E_{ii}^{\bar{x}_3}}{1-\nu_{ij}\nu_{ji}},\ q_{ij}^{\bar{x}_3} = \frac{\nu_{ji}E_{ii}^{\bar{x}_3}}{1-\nu_{ij}\nu_{ji}} = q_{ji}^{\bar{x}_3},\ q_{66}^{\bar{x}_3} = E_{ij}^{\bar{x}_3},\ (i,j=1,2)$$

The strains of inhomogeneous orthotropic double-curved shallow shells associated with the displacement field are as follows:

$$\begin{bmatrix} e_{11}^{0}\\ e_{22}^{0}\\ e_{12}^{0}\end{bmatrix} = \begin{bmatrix} \frac{\partial u_1}{\partial x_1} - \frac{u_3}{R_1} + \frac{1}{2}\left(\frac{\partial u_3}{\partial x_1}\right)^2\\ \frac{\partial u_2}{\partial x_2} - \frac{u_3}{R_2} + \frac{1}{2}\left(\frac{\partial u_3}{\partial x_2}\right)^2\\ \frac{\partial u_2}{\partial x_1} + \frac{\partial u_1}{\partial x_2} + \frac{\partial u_3}{\partial x_1}\frac{\partial u_3}{\partial x_2}\end{bmatrix} \tag{3}$$

The stress resultants and couples of inhomogeneous orthotropic double-curved shallow shells are defined by [1,13,16]:

$$(N_{ij}, M_{ij}) = \int_{-h/2}^{h/2} (1, x_3)\sigma_{ij}\mathrm{d}x_3,\ (i,j=1,2) \tag{4}$$

The stress function for the stress resultants defined by [1]:

$$(N_{11}, N_{22}, N_{12}) = h\left(\frac{\partial^2 F}{\partial x_2^2}, \frac{\partial^2 F}{\partial x_1^2}, -\frac{\partial^2 F}{\partial x_1 \partial x_2}\right) \tag{5}$$

By using relations (2), (4) and (5), and considering the condition of compatibility (Volmir [1]), which expressed in terms of u_3 and F, the equations of forced vibration of inhomogeneous double-curved shallow shells with a von Karman-type nonlinearity may be written as,

$$\begin{aligned} L_{11}(F) + L_{12}(u_3) + L_{13}(F,u_3) + q(t) &= D_{\rho}^{IH}\frac{\partial^2 u_3}{\partial t^2}\\ L_{21}(F) + L_{22}(u_3) + L_{13}(u_3,u_3) &= 0 \end{aligned} \tag{6}$$

where

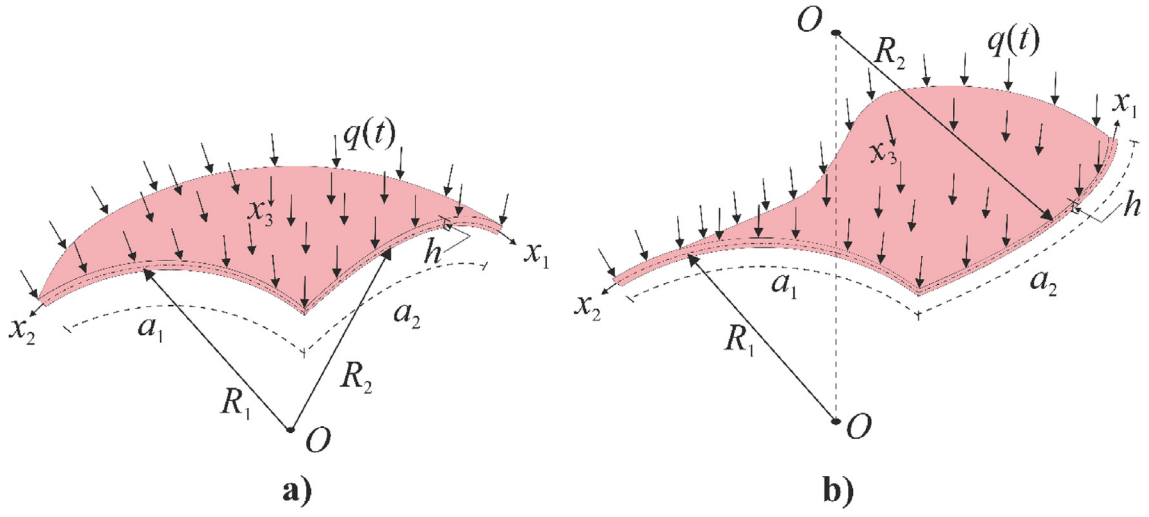

Fig. 1. Inhomogeneous orthotropic double-curved shallow shells under external excitation.

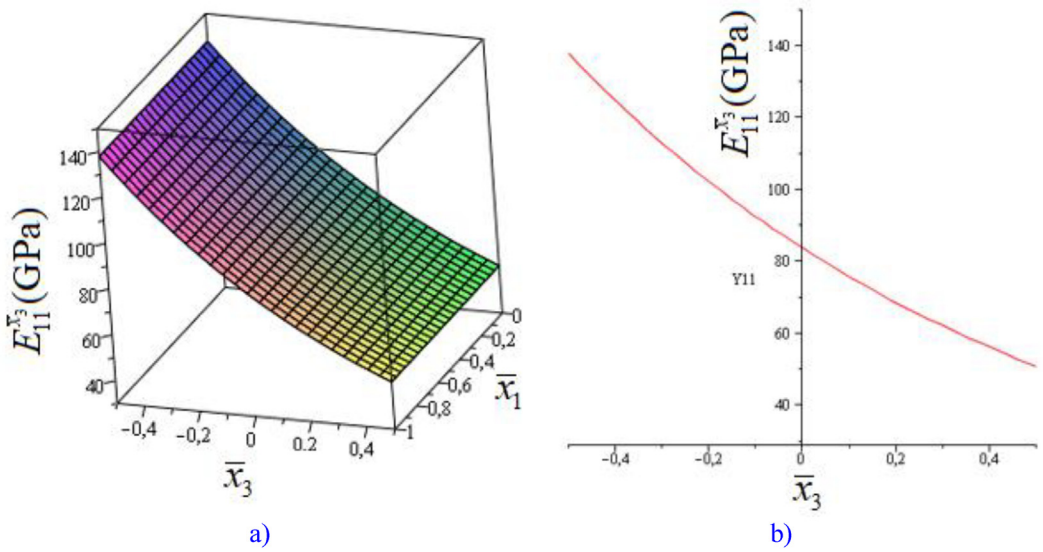

Fig. 2. Variation of $E_{11}^{\bar{x}_3}$ versus the thickness coordinate $\bar{x}_3$ in **(a)** three and **(b)** two-dimensional coordinate systems for $\eta_1 = -1$.

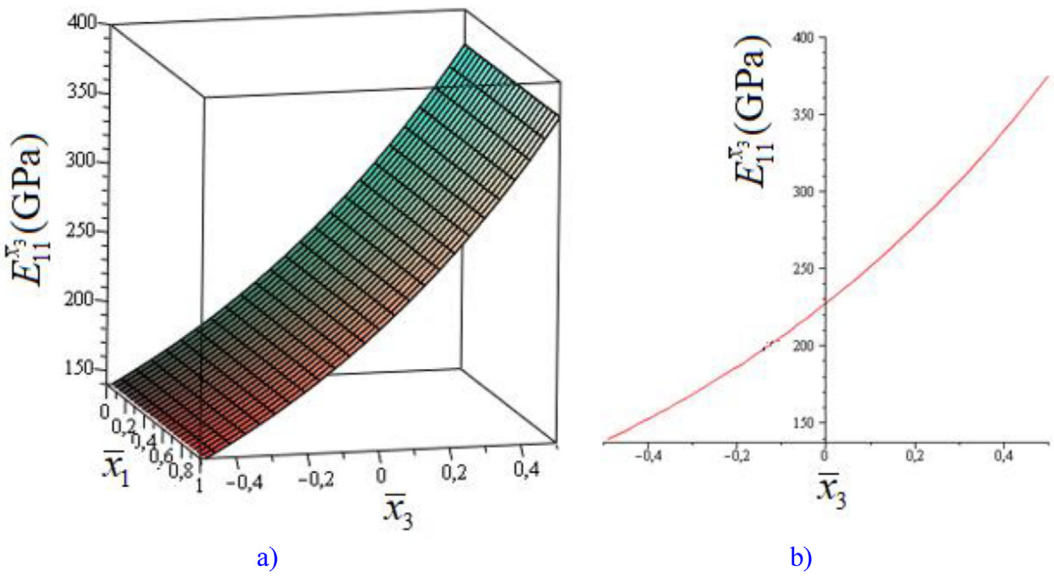

Fig. 3. Variation of $E_{11}^{\bar{x}_3}$ versus the thickness coordinate $\bar{x}_3$ in **(a)** three and **(b)** two-dimensional coordinate systems for $\eta_1 = +1$.

$$
\begin{aligned}
L_{11}(F) &= h\Big[C_{12}\tfrac{\partial^4}{\partial x_1^4} + (C_{11} - 2C_{31} + C_{22})\tfrac{\partial^4}{\partial x_1^2 \partial x_2^2} + C_{21}\tfrac{\partial^4}{\partial x_2^4} + \tfrac{1}{R_2}\tfrac{\partial^2}{\partial x_1^2} + \tfrac{1}{R_1}\tfrac{\partial^2}{\partial x_2^2}\Big],\\
L_{12}(u_3) &= -C_{13}\tfrac{\partial^4}{\partial x_1^4} - (C_{14} + 2C_{32} + C_{23})\tfrac{\partial^4}{\partial x_1^2 \partial x_2^2} - C_{24}\tfrac{\partial^4}{\partial x_2^4},\\
L_{13}(F, u_3) &= h\Big(\tfrac{\partial^2}{\partial x_1^2}\tfrac{\partial^2}{\partial x_2^2} - 2\tfrac{\partial^2}{\partial x_1 \partial x_2}\tfrac{\partial^2}{\partial x_1 \partial x_2} + \tfrac{\partial^2}{\partial x_1^2}\tfrac{\partial^2}{\partial x_2^2}\Big),\\
L_{21}(F) &= h\Big[B_{11}\tfrac{\partial^4}{\partial x_2^4} + (B_{12} + B_{21} + B_{31})\tfrac{\partial^4}{\partial x_1^2 \partial x_2^2} + B_{22}\tfrac{\partial^4}{\partial x_1^4}\Big],\\
L_{22}(u_3) &= -B_{23}\tfrac{\partial^4}{\partial x_1^4} - (B_{24} + B_{13} - B_{32})\tfrac{\partial^4}{\partial x_1^2 \partial x_2^2} - B_{14}\tfrac{\partial^4}{\partial x_2^4} + \Big(\tfrac{1}{R_2}\tfrac{\partial^2}{\partial x_1^2} + \tfrac{1}{R_1}\tfrac{\partial^2}{\partial x_2^2}\Big),\\
L_{23}(u_3, u_3) &= -\Big(\tfrac{\partial^2}{\partial x_1 \partial x_2}\Big)^2 + \tfrac{\partial^2}{\partial x_1^2}\tfrac{\partial^2}{\partial x_2^2}
\end{aligned}
\tag{7}
$$

where $D_\rho^{IH} = D_\rho^H \int_{-h/2}^{h/2} e^{\eta_2(\bar{x}_3+0.5)} dx_3 = hD_\rho^H(e^{\eta_2} - 1)$, $C_{ij}, B_{ij}(i,j = 1,2,\ldots,4)$ are defined in Appendix A. Note that the Karman geometric nonlinearity and linear operators are given in terms of $L_{ik}(\cdot,\cdot)$ and $L_{ij}(\cdot)$, $(i, j = 1,2, k = 3)$, respectively.

3. Solution procedure

The inhomogeneous orthotropic double-curved shallow shell obeys simply-supported boundary conditions, and presented as follows [1]:

$$
\begin{aligned}
&u_3 = 0, \quad \tfrac{\partial^2 u_3}{\partial x_1^2} = 0, \text{ at } x_1 = 0 \text{ and } x_1 = a_1\\
&u_3 = 0, \quad \tfrac{\partial^2 u_3}{\partial x_2^2} = 0, \text{ at } x_2 = 0 \text{ and } x_2 = a_2
\end{aligned}
\tag{8}
$$

The approximation function u_3 is sought as follows [1,19]:

$$u_3(x_1, x_2, t) = u_3(t)\,\sin(k_1 x_1)\,\sin(k_2 x_2) \tag{9}$$

where $k_1 = m\pi/a_1$, $k_2 = n\pi/a_2$, and $\bar{u}_3(t)$ is the function depending on the time.

Letting (9) in the second equation of (6), after integrating, one gets

$$F = l_1\bar{u}_3^2\cos(2k_1x_1) + l_2\bar{u}_3^2\cos(2k_2x_2) + l_3\bar{u}_3\sin(k_1x_1)\sin(k_2x_2) \tag{10}$$

where

$$l_1 = \frac{k_2^2}{32hk_1^2B_{22}},\ l_2 = \frac{k_1^2}{32hk_2^2B_{11}},\ l_3 = \frac{B_{23}k_1^4 + (B_{24}+B_{13}-B_{32})k_1^2k_2^2 + B_{14}k_2^4 + k_1^2/R_2 + k_2^2/R_1}{h\left(B_{11}k_2^4 + (B_{12}+B_{21}+B_{31})k_1^2k_2^2 + B_{22}k_1^4\right)} \tag{11}$$

By applying Galerkin method to the first equation of the set (6) and introducing (9) and (10) in this equation, and assuming that the external exciting load changes harmonically [1,2,14], i.e.,

$$q(t) = q_0\cos(\varphi t) \tag{12}$$

we obtain the nonlinear differential equation of forced vibration for inhomogeneous orthotropic double-curved shallow shells as follows:

$$\frac{d^2\bar{u}_3}{dt^2} + \omega_0^2\bar{u}_3 + Q_1\bar{u}_3^2 + Q_2\bar{u}_3^3 - Q_3q_0\cos(\varphi t) = 0 \tag{13}$$

where φ and q_0 indicate the frequency and amplitude of the external excitation, respectively, $\omega_L = \omega_0$ denotes the linear frequency for inhomogeneous orthotropic double-curved shallow shells and defined by,

$$\omega_0 = \frac{1}{\left(D_\rho^H\right)^{0.5}}\left\{\left[\frac{k_1^2}{R_2} + \frac{k_2^2}{R_1} - C_{12}k_1^4 - (C_{11} - 2C_{31} + C_{22})k_1^2k_2^2 - C_{21}k_2^4\right]hp_3 + C_{13}k_1^4 + (C_{14} + 2C_{32} + C_{24})k_1^2k_2^2 + C_{24}k_2^4\right\}^{0.5} \tag{14}$$

in which

$$Q_1 = \frac{8h\gamma_{mn}}{3D_\rho^H}\frac{8C_{12}k_1^4l_1 + 8C_{21}k_2^4l_2 - k_1^4k_2^2l_3 - 2l_1k_1^2/R_2 - 2l_2k_2^2/R_1}{a_1a_2k_1k_2},\ Q_2 = \frac{2hk_1^2k_2^2(l_1+l_2)}{D_\rho^H},\ Q_3 = \frac{4\gamma_{mn}}{D_\rho^Ha_1a_2k_1k_2},\ \gamma_{mn} = \left[1 - (-1)^m - (-1)^n + (-1)^{m+n}\right] \tag{15}$$

As can be seen, the equation of motion (13) is an inhomogeneous differential equation and the external excitation, which is a harmonic function $q(t)$, is the non-homogeneous term of this equation. Let's write the Eq. (13) in the following form:

$$\frac{d^2\bar{u}_3}{dt^2} + \omega_0^2\bar{u}_3 = -Q_{11}\varepsilon\bar{u}_3^2 - Q_{21}\varepsilon^2\bar{u}_3^3 + Q_{31}\varepsilon^2\cos(\varphi t) \tag{16}$$

where the following definitions apply:

$$Q_{11} = \frac{Q_1}{\varepsilon},\ Q_{21} = \frac{Q_2}{\varepsilon^2},\ Q_{31} = \frac{Q_3q_0}{\varepsilon^2} \tag{17}$$

The initial conditions are given as [2]:

$$\bar{u}_3\Big|_{t=0} = \bar{u}_{3\max},\ \frac{d\bar{u}_3}{dt}\Big| = 0 \tag{18}$$

As it is known, in the case of primary resonance, assuming that the frequency of the external excitation φ and the frequency ω_0 for the linear vibration are very close to each other, the correlation between φ and ω_0 is used as a detuning parameter σ:

$$\varphi = \omega_0 + \varepsilon^2\sigma \tag{19}$$

where $\sigma = O(1)$. The Eq. (16) is solved by a perturbation method using multiple time scales. When this method is applied to the solution Eq. (16), we sought the solution in terms of different scales by

$$\bar{u}_3(t,\varepsilon) = u_{03}(\tau_0,\tau_1,\tau_2) + \varepsilon u_{13}(\tau_0,\tau_1,\tau_1) + \varepsilon^2u_{13}(\tau_0,\tau_1,\tau_1)... \tag{20}$$

where $\tau_0 = t$, $\tau_1 = \varepsilon t$ and $\tau_2 = \varepsilon^2 t$. Furthermore, the excitation in terms τ_0 and τ_2 can be expressed as,

$$\varphi t = \omega\tau_0 + \sigma\tau_2 \tag{21}$$

Introducing of (20) and (21) into (16) and equating the coefficients of $\varepsilon^i(i = 0,1,2)$, one gets

$$D_0^2\bar{u}_{03} + \omega_0^2\bar{u}_{03} = 0 \tag{22}$$

$$D_0^2\bar{u}_{13} + \omega_0^2\bar{u}_{13} = -2D_0D_1\bar{u}_{03} - Q_1\bar{u}_{03}^2 \tag{23}$$

$$D_0^2\bar{u}_{23} + \omega_0^2\bar{u}_{23} = -2D_0D_1\bar{u}_{13} - 2D_0D_2\bar{u}_{03} - D_1^2\bar{u}_{03} \mu_1D_0\bar{u}_{03} - 2Q_1\bar{u}_{03}\bar{u}_{13} - Q_2\bar{u}_{03}^3 + Q_{31}\cos(\omega_0\tau_0 + \sigma\tau_2) \tag{24}$$

Here the following derivatives are used:

$$\frac{d}{dt} = \frac{d\tau_0}{dt}\frac{\partial}{\partial\tau_0} + \frac{d\tau_1}{dt}\frac{\partial}{\partial\tau_1} + ... = D_0 + \varepsilon D_1 + ...$$
$$\frac{d^2}{dt^2} = D_0^2 + 2\varepsilon D_0D_1 + \varepsilon^2(D_1^2 + 2D_0D_2) + ... \tag{25}$$

It can be easily seen that the general solution of the Eq. (22) is as follows:

$$\bar{u}_{03} = c_1(\tau_1,\tau_2)e^{i\omega_0\tau_0} + c_2(\tau_1,\tau_2)e^{-i\omega_0\tau_0} \tag{26}$$

where $c_1(\tau_1,\tau_2)$ and $c_2(\tau_1,\tau_2)$ are integral constants. Substituting (26) into Eq. (23), we obtain,

$$D_0^2\bar{u}_{13} + \omega_0^2\bar{u}_{13} = -c_1\left[2i\omega_0D_1e^{i\omega_0\tau_0} + Q_{21}\left(c_1e^{2i\omega_0\tau_0} + c_2\right)\right] + c_3 \tag{27}$$

Eliminating the terms from Eq. (27) that procedure secular terms in $\bar{u}_{13}$ gives $D_1c_1 = 0$ or $c_1 = c_1(\tau_2)$. Thus, the solution of Eq. (27) is as follows:

$$\bar{u}_{13} = \frac{Q_{11}\left(-6c_1c_2 + c_1^2e^{2i\omega_0\tau_0} + c_2^2e^{-2i\omega_0\tau_0}\right)}{3\omega_0^2} \tag{28}$$

Substituting expressions (26) and (28) into Eq. (24), yields

$$D_0^2\bar{u}_{23} + \omega_0^2\bar{u}_{23} = -\left[2i\omega_0\mu_1c_1 + \left(3Q_{21} - \frac{10Q_{11}^2}{3\omega_0^2}\right)c_1^2c_2 - 0.5Q_{31}e^{i\sigma\tau_2}\right]e^{i\omega_0\tau_0} + c_3 + nst \tag{29}$$

where c_3 is stands for the complex conjugate of the preceding terms, the prime denotes the derivatives with respect to τ_2 and *nst* stands for terms proportional to $e^{\pm3i\omega_0\tau_0}$ [2].

Let us equate the secular terms in the Eq. (29) to zero:

$$2i\omega_0\frac{dc_1}{d\tau_2} + \left(3Q_{21} - \frac{10Q_{11}^2}{3\omega_0^2}\right)c_1^2c_2 - 0.5Q_{31}e^{i\sigma\tau_2} = 0 \tag{30}$$

Let's write c_1 in polar form, that is $c_1 = 0.5\alpha e^{i\beta}$, and substituting this expression into Eq. (30), separating its real and imaginary parts, one gets

$$\alpha' = \frac{Q_{31}}{2\omega_0}\sin\psi \tag{31}$$

$$a\beta' = \frac{1}{8\omega_0}\left(3Q_{21} - \frac{10Q_{11}^2}{3\omega_0^2}\right)\alpha^3 - \frac{Q_{31}}{2\omega_0}\cos\psi \tag{32}$$

where α and β indicate the amplitude and phase and are real, and γ denotes the new phase angle and expressed as:

$$\psi = \sigma\tau_2 - \beta \tag{33}$$

If eliminating β from Eqs. (32) and (33), the result is

$$\alpha\frac{d\psi}{d\tau_2} = \alpha\sigma - \frac{1}{8\omega_0}\left(3Q_{21} - \frac{10Q_{11}^2}{3\omega_0^2}\right)\alpha^3 + \frac{Q_{31}}{2\omega_0}\cos\psi \tag{34}$$

At steady state, using symbol $\alpha = hA_\Delta$ from Eqs. (31) and (34), the frequency-response equation for inhomogeneous orthotropic double-curved shallow shells follows immediately:

$$\sigma_j = \frac{h^2A_\Delta^2}{8\omega_0}\left(3Q_{21} - \frac{10Q_{11}^2}{3\omega_0^2}\right) \mp \frac{Q_{31}}{2hA_\Delta\omega_0},\ (j = 1,2) \tag{35}$$

where A_Δ is the dimensionless amplitude.

The equation of the nondimensional large amplitude forced vibration frequency of inhomogeneous orthotropic double-curved shallow shells in the first resonance state is found as follows:

$$\varphi_{jLA}^{forc} = (\omega_0 + \varepsilon^2\sigma_j)h\sqrt{D_\rho^H/Y_{11}^H}\ (j = 1,2) \tag{36}$$

The large amplitude forced vibration frequency to linear forced vibration frequency ($\varphi_{jLA}^{forc}/\omega_L$) for inhomogeneous orthotropic double-curved shallow shells in the first resonance state is found as follows

$$\varphi_{jLA}^{forc}/\omega_L = \left(1+\varepsilon^2\sigma_j\omega_0^{-1}\right)\ (j=1,2) \tag{37}$$

From Eq. (36), the expression for the backbone curve ϖ_{LA}^{Bbone} and $\varpi_{LA}^{Bbone}/\omega_L$ for inhomogeneous orthotropic double-curved shallow shells we obtain, as $q_0 = 0$.

4. Results and discussion

4.1. Numerical verification

To verify current results, $\varpi_{LA}^{Bbone}/\omega_L$ for homogenous orthotropic shells are compared with the results of Sheng and Wang [15] (see, Table 1). The ϖ_{LA}^{Bbone} is expressed as $\varpi_{LA}^{Bbone} = \omega_L + \varepsilon^2\sigma_1$, in which the σ_1 is found by setting $Q_{31} = 0$ (without excitation) and $a_2 = \pi R_2$ in the Eq. (36). The HOM properties for $\eta_i = 0$ $(i = 1,2)$ and shell parameters are: $a_2 = 1.575R_1$, $h/R_1 = 0.01$, $Y_{11}^H = 2\times10^{11}(\mathrm{N/m^2})$, $\mathrm{Y_{22}^H = Y_{12}^H} = 10^{11}(\mathrm{N/m^2})$, $\nu_{12} = 1/5$ and $D_\rho^H = 7.8\times10^3\,\mathrm{kg/m^3}$. It has been observed that our results coincide with the results of the comparative study.

In Table 2, the values of ω_L for homogenous orthotropic pates are compared with the results of Thai and Kim [22]. Considering $R_1 = R_2 \to \infty$ in Eq. (14), the expression of linear frequency is transformed to the expression of homogenous orthotropic plates. The data used for numerical calculations are as follows: $Y_{11}^H/Y_{22}^H = 25,\ 40$; $G_{12}^H = 0.5Y_{22}^H$, $\nu_{12} = 0.25$, $D_\rho^H = 1$, $a_1/a_2 = 1$ and $a_1/h = 100$. The coincidence of the comparison results presented in Table 2 is one of the indicators of the correctness of expressions for frequencies which obtained in our study.

4.2. New forced vibration analysis

The unique numerical analysis on the $\varphi_{LA}^{forc_j}/\omega_L (j=1,2)$ for homogenous and inhomogeneous orthotropic shallow spherical and hyperbolic paraboloidal (or hypar) shells are presented under this subheading. The orthotropic material used in the formation of shallow shell is graphite/epoxy and its properties are as follows [23]:

$$Y_{11}^H = 137.9\times10^9(\mathrm{N/m^2}),\ \mathrm{Y_{22}^H} = 8.96\times10^9(\mathrm{N/m^2}),\ \mathrm{Y_{12}^H} = 7.1\times10^9(\mathrm{N/m^2}),$$
$$\nu_{12} = 0.3, \nu_{21} = \nu_{12}Y_{22}^H/Y_{11}^H,\ D_\rho^H = 1450(\mathrm{kg/m^3})$$

The shallow shell parameters, $a_1/h = 20,\ 30,\ 35,\ 40$; $a_1/a_2 = 0.5,\ 1.0,\ 1.5$; $R_1/a_1 = 1,\ 3,\ 5$ and various modes (m,n) are considered. In all tables and figures, except Fig. 3 use the following expression for external excitation: $q_0 = A_{q_0}h^2D_\rho^H\omega_0^2$ in which the amplitude of the external excitation is considered as $A_{q_0} = 4\times10^{-3}$ (Sheng and Wang [15]) The nondimensional amplitude A_Δ changes from 0.06 to 1.06 with 0.1 or 0.2 steps. The $\varphi_{LA}^{forc_j}$ and $\varphi_{LA}^{forc_j}/\omega_L (j=1,2)$ represent the first and second components of the forced vibration frequency and frequncies ratio, respectively, ϖ_{LA}^{Bbone} and $\varpi_{LA}^{Bbone}/\omega_L$ represent the backbone curve and frequncies ratio at $q_0 = 0$. The inhomogeneity coefficients that characterize the variations of density, Young and shear moduli are considered as: $(\eta_1,\eta_2) = (-1,0)$ or $\mathrm{IH_1}$, $(\eta_1,\eta_2) = (-1,-1)$ or $\mathrm{IH_2}$, $(\eta_1,\eta_2) = (1,0)$ or $\mathrm{IH_3}$ and $(\eta_1,\eta_2) = (1,1)$ or $\mathrm{IH_4}$. In the figures and tables, $R_2/R_1 = 1$ refers to the spherical shell and $R_2/R_1 = -1$ refers to the hypar shell. Also, in all tables and graphs, magnitudes of $\varphi_{LA}^{forc_j}$ are written by multiplying by 1000. The backbone is abbreviated as Bbone in all figures.

Table 1
Comparison of variation of $\varpi_{LA}^{Bbone}/\omega_L$ for homogenous orthotropic shell according to A_Δ at $(m,n) = (1,4)$.

A_Δ	Sheng and Wang [14]	Present
0.5	1.0017	1.00185
1.0	1.0066	1.00738
1.5	1.0149	1.01654
2.0	1.0265	1.02923
2.5	1.0414	1.04531

Table 2
Comparison the $\omega_{1L} = \omega_L(a_1^2/h)\sqrt{D_\rho^H/Y_{22}^H}$ for homogenous orthotopic plates.

	Thai and Kim [20]	Present study
Y_{11}^H/Y_{22}^H	$\omega_{1L} = \omega_L(a_1^2/h)\sqrt{D_\rho^H/Y_{22}^H}$	
25	15.1972	15.2278
40	18.7462	18.8052

The distributions of $\varphi_{LA}^{forc_j}(j=1,2)$ and ϖ_{LA}^{Bbone} for homogenous, and inhomogeneous-shallow spherical and hypar shells depending on the A_Δ with $a_1/h =$ 30, 35, 40; $a_1/a_2 = 1$; $R_1/a_1 = 3$ and $(m,n) = (1,1)$, are presented in Tables 3 and 4. As can be seen from Tables 3 and 4, the values of the large amplitude forced vibration frequency for the inhomogeneous orthotropic spherical shells are higher than the than those in the inhomogeneous orthotropic hypar shells. Also, the values of large amplitude forced vibration frequency exhibit different manners for inhomogeneous shallow spherical and hypar shells depending on the increasing of A_Δ. The $\varphi_{LA}^{forc_1}$ and ϖ_{LA}^{Bbone} values for the inhomogeneous shallow spherical shell decrease, while the curve of $\varphi_{LA}^{forc_2}$ first increases and then decreases due to the increase of A_Δ with all a_1/h ratio and for all inhomogeneity profiles. The values of $\varphi_{LA}^{forc_1}$ and ϖ_{LA}^{Bbone} for the inhomogeneous shallow hypar shell increase due to the increase of A_Δ with all inhomogeneity profiles, while the magnitudes of $\varphi_{LA}^{forc_2}$ reduces first and then increments for $a_1/h < 40$. The values of large amplitude forced vibration frequency for inhomogeneous shallow spherical and hypar shells consisting of $\mathrm{IH_3}$ profile are higher than those in homogenous-shallow shells, while those values for inhomogeneous shallow spherical and hypar shells consisting of the $\mathrm{IH_1}$ profile are lower than the large amplitude forced vibration frequency values for the homogenous shells. In addition, the large amplitude forced vibration frequency values for inhomogeneous shallow spherical and hypar shells consisting of $\mathrm{IH_2}$ and $\mathrm{IH_4}$ profiles are very close to those in the homogenous shells.

The effect of inhomogeneity profiles on the large amplitude forced vibration frequency values of inhomogeneous shallow spherical and hypar shells increases for the $\mathrm{IH_1}$ profile, whereas decreases for $\mathrm{IH_3}$ profile. For example, the effect of $\mathrm{IH_1}$ profile increases from (-21.43%) to (-21.58%) for inhomogeneous shallow spherical and decreases from (–22.43%) to (-21.53%) for inhomogeneous shallow hypar shell, when A_Δ increases from 0.06 to 0.66. Morever, the effects of the $\mathrm{IH_3}$ profile decrease from (29.54%) to (29.29%) and from (27.89%) to (27.72%) for inhomogeneous shallow spherical and hypar shells, respectively. Although the effects of $\mathrm{IH_2}$ and $\mathrm{IH_4}$ profiles on the values of the large amplitude forced vibration frequency for inhomogeneous shallow spherical and hypar shells are smaller, it increases or decreases depending on the increase of the A_Δ. For example, the effects of the $\mathrm{IH_2}$ profile on $\varphi_{LA}^{forc_1}$ and ϖ_{LA}^{Bbone} for the inhomogeneous shallow spherical shell increase from (-0.68%) to (-1.19%) and from (-1.17%) to (-1.37%), respectively, while its effect on the $\varphi_{LA}^{forc_2}$ decreases from (-3.16%) to (-1.55%), as A_Δ increases from 0.06 to 0.66. The effects of the $\mathrm{IH_4}$ profile on the values of $\varphi_{LA}^{forc_2}$ and ϖ_{LA}^{Bbone} increase from (-0.25%) to (-1.24%) and from (-1.17%) to (-1.37%), respectively, while its effect on the $\varphi_{LA}^{forc_1}$ decreases from (-2.51%) to (-1.50%). Again, when A_Δ increases from 0.06 to 0.66, the effects of the $\mathrm{IH_2}$ profile on $\varphi_{LA}^{forc_1}$ and ϖ_{LA}^{Bbone} for inhomogeneous

Table 3
Variation of large amplitude forced vibration frequency and backbone curve of homogenous and in homogenous shperical shells according to A_Δ for different a_1/h.

a_1/h	A_Δ	$\varphi_{LA}^{forc_j} \times 10^3 (j=1,2)$ for spherical shells								
		$(\eta_1,\eta_2)=(0,0)$ or HO			$(\eta_1,\eta_2)=(-1,0)$ or IH_1			$(\eta_1,\eta_2)=(-1,-1)$ or IH_2		
		$\varphi_{LA}^{forc_1}$	$\varphi_{LA}^{forc_2}$	ϖ_{LA}^{Bbone}	$\varphi_{LA}^{forc_1}$	$\varphi_{LA}^{forc_2}$	ϖ_{LA}^{Bbone}	$\varphi_{LA}^{forc_1}$	$\varphi_{LA}^{forc_2}$	ϖ_{LA}^{Bbone}
30	0.06	5.390	5.042	5.216	4.235	3.962	4.099	5.427	4.883	5.155
	0.26	5.244	5.163	5.203	4.119	4.056	4.087	5.204	5.078	5.141
	0.46	5.197	5.152	5.175	4.080	4.044	4.062	5.145	5.074	5.109
	0.66	5.146	5.114	5.130	4.035	4.010	4.023	5.085	5.035	5.060
35	0.06	4.313	4.034	4.173	3.395	3.176	3.285	4.350	3.914	4.132
	0.26	4.192	4.128	4.160	3.299	3.249	3.274	4.168	4.067	4.118
	0.46	4.148	4.111	4.130	3.262	3.234	3.248	4.114	4.057	4.085
	0.66	4.095	4.070	4.082	3.218	3.198	3.208	4.055	4.015	4.035
40	0.06	3.588	3.357	3.472	2.829	2.646	2.738	3.625	3.262	3.443
	0.26	3.487	3.433	3.460	2.748	2.706	2.727	3.472	3.388	3.430
	0.46	3.447	3.417	3.432	2.716	2.692	2.704	3.425	3.377	3.401
	0.66	3.399	3.378	3.389	2.676	2.660	2.668	3.372	3.339	3.356
		$(\eta_1,\eta_2)=(1,0)$ or IH_3			$(\eta_1,\eta_2)=(1,1)$ or IH_4					
a_1/h	A_Δ	$\varphi_{LA}^{forc_1}$	$\varphi_{LA}^{forc_2}$	ϖ_{LA}^{Bbone}	$\varphi_{LA}^{forc_1}$	$\varphi_{LA}^{forc_2}$	ϖ_{LA}^{Bbone}	$R_2=R_1$, $a_1/a_2=1$, $R_1/a_1=3$		
30	0.06	6.983	6.532	6.757	5.255	5.055	5.155			
	0.26	6.791	6.687	6.739	5.164	5.118	5.141			
	0.46	6.727	6.668	6.697	5.122	5.096	5.109			
	0.66	6.653	6.612	6.633	5.069	5.051	5.060			
35	0.06	5.597	5.236	5.417	4.212	4.052	4.132			
	0.26	5.439	5.356	5.398	4.136	4.099	4.118			
	0.46	5.379	5.332	5.355	4.096	4.075	4.085			
	0.66	5.305	5.272	5.289	4.042	4.027	4.035			
40	0.06	4.664	4.363	4.514	3.510	3.377	3.443			
	0.26	4.531	4.462	4.497	3.446	3.415	3.430			
	0.46	4.478	4.439	4.458	3.410	3.392	3.401			
	0.66	4.412	4.385	4.399	3.362	3.349	3.356			

Table 4
Variation of large amplitude forced vibration frequency and backbone curve of homogenous and inhomogenous hypar shells according to A_Δ for different a_1/h.

a_1/h	A_Δ	$\varphi_{LA}^{forc_j} \times 10^3 (j=1,2)$ for hypar shells								
		$(\eta_1,\eta_2)=(0,0)$ or HO			$(\eta_1,\eta_2)=(-1,0)$ or IH_1			$(\eta_1,\eta_2)=(-1,-1)$ or IH_2		
		$\varphi_{LA}^{forc_1}$	$\varphi_{LA}^{forc_2}$	ϖ_{LA}^{Bbone}	$\varphi_{LA}^{forc_1}$	$\varphi_{LA}^{forc_2}$	ϖ_{LA}^{Bbone}	$\varphi_{LA}^{forc_1}$	$\varphi_{LA}^{forc_2}$	ϖ_{LA}^{Bbone}
30	0.06	3.754	3.512	3.633	2.912	2.724	2.818	3.732	3.358	3.545
	0.26	3.681	3.625	3.653	2.855	2.812	2.833	3.607	3.520	3.564
	0.46	3.714	3.682	3.698	2.879	2.854	2.867	3.630	3.581	3.606
	0.66	3.779	3.757	3.768	2.927	2.910	2.919	3.688	3.654	3.671
35	0.06	2.758	2.580	2.669	2.139	2.001	2.070	2.741	2.467	2.604
	0.26	2.695	2.654	2.675	2.090	2.058	2.074	2.640	2.576	2.608
	0.46	2.700	2.676	2.688	2.090	2.072	2.081	2.636	2.600	2.618
	0.66	2.717	2.701	2.709	2.100	2.087	2.093	2.646	2.621	2.633
40	0.06	2.111	1.975	2.043	1.637	1.532	1.585	2.098	1.888	1.993
	0.26	2.055	2.024	2.040	1.593	1.568	1.581	2.012	1.964	1.988
	0.46	2.041	2.024	2.032	1.579	1.565	1.572	1.991	1.963	1.977
	0.66	2.027	2.015	2.021	1.563	1.553	1.558	1.969	1.950	1.959
		$(\eta_1,\eta_2)=(1,0)$ or IH_3			$(\eta_1,\eta_2)=(1,1)$ or IH_4			$R_2=-R_1$, $a_1/a_2=1$, $R_1/a_1=3$		
30	0.06	4.801	4.492	4.647	3.614	3.476	3.545			
	0.26	4.707	4.635	4.671	3.579	3.548	3.564			
	0.46	4.747	4.706	4.726	3.615	3.597	3.606			
	0.66	4.826	4.798	4.812	3.677	3.665	3.671			
35	0.06	3.527	3.299	3.413	2.654	2.553	2.604			
	0.26	3.445	3.393	3.419	2.620	2.596	2.608			
	0.46	3.446	3.417	3.432	2.624	2.611	2.618			
	0.66	3.462	3.441	3.452	2.638	2.629	2.633			
40	0.06	2.700	2.525	2.613	2.032	1.954	1.993			
	0.26	2.626	2.586	2.606	1.997	1.979	1.988			
	0.46	2.603	2.580	2.591	1.982	1.972	1.977			
	0.66	2.576	2.560	2.568	1.963	1.956	1.959			

hypar shell increase from (-0.60%) to (-2.40%) and from (-2.43%) to (-2.56%), respectively, whereas its effect on the $\varphi_{LA}^{forc_2}$ decreases from (−4.39%) to (−2.73%). Similarly, the effects of the IH_4 profile on $\varphi_{LA}^{forc_2}$ and ϖ_{LA}^{Bbone} increase from (−1.03%) to (−2.45%) and from (−2.43%) to (−2.56%), whereas its effect on the values of $\varphi_{LA}^{forc_1}$ decrease from (−3.75%) to (−2.68%). Due to the increase of a_1/h, the values of large amplitude forced vibration frequency for inhomogeneous shallow spherical and hypar shells decrease approximately 0.4%

for all inhomogenety profiles except the IH_3 profile, while they increase approximately 0.5% and 0.7%, respectively, at the IH_3 profile.

The values of $\varphi_{LA}^{forc_1}$, $\varphi_{LA}^{forc_2}$ and ϖ_{LA}^{Bbone} for spherical and hypar shells consisting of homogenous and inhomogeneous orthotropic materials changes depending on the A_Δ with different R_1/a_1 are shown in Fig. 4 and Table 5. Depending on the increase of A_Δ, the values of $\varphi_{LA}^{forc_1}$ first decreases and then increases, while $\varphi_{LA}^{forc_2}$ and ϖ_{LA}^{Bbone} increase for inhomogeneous orthotropic shallow spherical and hypar shells. For a fixed A_Δ, the values of $\varphi_{LA}^{forc_1}$, $\varphi_{LA}^{forc_2}$ and ϖ_{LA}^{Bbone} decrease for both spherical and hypar shells, and this decrease rate turns out to be greater for the inhomogeneous orthotropic shallow spherical shell depending on the increase of R_1/a_1. When comparing large amplitude forced vibration frequency of inhomogeneous orthotropic shallow spherical and hypar shells with each other, the influence of the IH_1 profile on $\varphi_{LA}^{forc_1}$, $\varphi_{LA}^{forc_2}$ and ϖ_{LA}^{Bbone} for the spherical shell is 0.4% greater than for the hypar shell. In addition, depending on the increase of R_1/a_1, the change of the influence of the IH_1 profile is less than 1% for both shallow shells (see, Table 5).

In Fig. 5 and Table 6 plotted the changes of $\varphi_{LA}^{forc_1}$, $\varphi_{LA}^{forc_2}$ and ϖ_{LA}^{Bbone} for homogenous and inhomogeneous orthotropic shallow spherical and hipar shells which are made of the IH_3 profile depending on the A_Δ ratio with $q_0 = 2\times10^5, 3\times10^5, 4\times10^5$, $a_1/a_2 = 1$, $R_1/a_1 = 3$, $a_1/h = 20$ and $(m = 1, n = 1)$. It is seen that the magnitudes of $\varphi_{LA}^{forc_1}$ and ϖ_{LA}^{Bbone} of inhomogeneous orthotropic shallow spherical shells reduce, while magnitudes of $\varphi_{LA}^{forc_2}$ increase to the maximum values and then decrease depending on the A_Δ for the fixed value of q_0. The values of $\varphi_{LA}^{forc_1}$ decrease to the minimum values and then increase, while $\varphi_{LA}^{forc_2}$ and ϖ_{LA}^{Bbone} increasing regularly for inhomogeneous shallow hypar shells. It is observed that this rate of increase (or decrease) is greater in the inhomogeneous shallow spherical shells compared to inhomogeneous shallow hypar shells for large values of q_0. Additionally, $\varphi_{LA}^{forc_1}$ and $\varphi_{LA}^{forc_2}$ increase for both inhomogeneous shallow spherical and hypar shells depending on the increase of q_0 for fixed A_Δ. This rate of increase becomes more significant at lower A_Δ. Although the effect of the IH_3 profile on $\varphi_{LA}^{forc_1}$ and $\varphi_{LA}^{forc_2}$ for both inhomogeneous shalow shells decreases with increasing A_Δ, it also increases with increasing q_0. In addition, when inhomogeneous shallow spherical and hypar shells are compared with each other, the influence of the IH_3 profile on $\varphi_{LA}^{forc_1}$ and $\varphi_{LA}^{forc_2}$ is greater with the inhomogeneous shallow hypar shell, and the difference of the inhomogeneity effect between the two shallow shells is increment due to the increase of excitation amplitude, q_0. For example, if q_0 increases from 2×10^5 to 4×10^5, the difference of the inhomogeneity effect between inhomogeneous shallow spherical and hypar shells increases from about (4.7%) to about (6.1%) for the IH_3 profile, at $A_\Delta = 0.06$ (se, Table 6).

The variation of $\varphi_{LA}^{forc_1}/\omega_L$, $\varphi_{LA}^{forc_2}/\omega_L$ and $\varpi_{LA}^{Bbone}/\omega_L$ ratios for inhomogeneous shallow spherical and hypar shells, consisting of IH_2, depending on the A_Δ with $R_1/a_1 = 1, 3, 5$, $a_1/a_2 = 1$, $a_1/h = 20$ and $(m, n) = (1, 1)$ are plotted in Fig. 6 and Table 7. As can be seen from Fig. 6 and Table 7, the $\varphi_{LA}^{forc_1}/\omega_L$ ratio for inhomogeneous shallow spherical and hypar shells reduces, taking on a minimum value, and then increase, while the $\varphi_{LA}^{forc_2}/\omega_L$ and $\varpi_{LA}^{Bbone}/\omega_L$ ratios continuously increase depending on the increase of A_Δ, as the $R_1/a_1 > 1$. The $\varphi_{LA}^{forc_2}/\omega_L$ ratio decreases to a minimum value and then increases, while the $\varphi_{LA}^{forc_1}/\omega_L$ and $\varpi_{LA}^{Bbone}/\omega_L$ ratios decrease continuously for both inhomogeneous shallow spherical and hypar shells, at $R_1/a_1 = 1$. In addition, from Fig. 6 and Table 7, there is an increase of $\varphi_{LA}^{forc_1}/\omega_L$, $\varphi_{LA}^{forc_2}/\omega_L$ and $\varpi_{LA}^{Bbone}/\omega_L$ due to an increase in R_1/a_1. When the inhomogeneous shallow spherical and hypar shells are compared with each other, the highest ratio of nonlinear to linear frequencies occur in inhomogeneous hypar shells for $R_1/a_1 > 1$ and in inhomogeneous spherical shells for $R_1/a_1 = 1$.

The variations of $\varphi_{LA}^{forc_1}/\omega_L$, $\varphi_{LA}^{forc_2}/\omega_L$ and $\varpi_{LA}^{Bbone}/\omega_L$ of inhomogeneous shallow spherical and inhomogeneous shallow hypar shells made of IH_4 depending on the A_Δ for different wave numbers (m, n) and with $a_1/a_2 = 1.5$; $R_1/a_1 = 1$; $a_1/h = 30$ are presented in Figs. 7 and 8. As can be seen from Figs. 7 and 8, when inhomogeneous shallow spherical and hypar shells are compared among themselves, the frequency ratio for the inhomogeneous shallow hypar shell is greater than the frequency ratio for the inhomogeneous shallow spherical shell. In addition, it is seen that the ratios of $\varphi_{LA}^{forc_1}/\omega_L$, $\varphi_{LA}^{forc_2}/\omega_L$ and $\varpi_{LA}^{Bbone}/\omega_L$ increase, as the wave numbers (m, n) increase, and it should be emphasized that the frequency ratios are more pronounced at $n = 1$ and as m increases. The ratios $\varphi_{LA}^{forc_2}/\omega_L$ and $\varpi_{LA}^{Bbone}/\omega_L$ for both inhomogeneous shallow spherical and hypar shells increase, while the ratio $\varphi_{LA}^{forc_1}/\omega_L$ decreases and take its minimum value, then increases again depending on the increase of A_Δ ratio.

The variations of $\varphi_{LA}^{forc_1}/\omega_L$, $\varphi_{LA}^{forc_2}/\omega_L$ and $\varpi_{LA}^{Bbone}/\omega_L$ of inhomogeneous shallow spherical and hypar shells made of IH_3 depending on the A_Δ for different $Y_{11}^H/Y_{22}^H = 10, 20, 50$ and with $a_1/a_2 = 1$; $R_1/a_1 = 3$; $a_1/h = 30$ and $(m, n) = (1, 1)$ are presented in Fig. 9 and Table 8. The $\varphi_{LA}^{forc_1}/\omega_L$ and $\varpi_{LA}^{Bbone}/\omega_L$ ratios for inhomogeneous shallow spherical shell decrease, while the ratio $\varphi_{LA}^{forc_2}/\omega_L$ decreases by taking its minimum value and then increases depending on the increase of A_Δ. The $\varphi_{LA}^{forc_2}/\omega_L$ and $\varpi_{LA}^{Bbone}/\omega_L$ ratios increase, while $\varphi_{LA}^{forc_1}/\omega_L$ ratio first reduces and then increments after taking its lowest value for the inhomogeneous shallow hypar shell depending on the increase of A_Δ. This kind of change (increase or decrease) is faster for the inhomogeneous orthotropic shallow spherical shell at the small values of the Y_{11}^H/Y_{22}^H ratio. The frequency ratio for the inhomogeneous orthotropic shallow spherical shell increases, while those decreases for the inhomogeneous orthotropic hypar shallow shell with the increasing of the Y_{11}^H/Y_{22}^H.

5. Conclusions

In this work, the large amplitude forced vibration of inhomogeneous orthotropic shallow spherical and hypar shells under external excitations is investigated. The mathematical model of inhomogeneous orthotropic double-curved shallow shells is built using the Hamilton principle and von Karman-type nonlinearity. Basic differential equations are reduced to ordinary differential equations using the Galerkin procedure. The frequency-amplitude relations of inhomogeneous orthotropic double-curved shallow shells and the nonlinear frequency response of forced vibrations are obtained using the multiscale method.

Numerical analysis reveals the following generalized results:

a) The values of large amplitude forced vibration frequency exhibit different manners for inhomogeneous shallow spherical and hypar shells depending on the increasing of nondimensional amplitude.
b) The $\varphi_{LA}^{forc_1}$ and ϖ_{LA}^{Bbone} values for the inhomogeneous shallow spherical shell decrease, while the curve of $\varphi_{LA}^{forc_2}$ first increases and then decreases due to the increase of nondimensional amplitude with all a_1/h ratio and for all inhomogeneity profiles.
c) The values of large amplitude forced vibration frequency for inhomogeneous shallow spherical and hypar shells consisting of IH_3 profile are higher than those in homogenous-shallow shells, while those values for IH_1 profile are lower than those in the homogenous shells.
d) The values of large amplitude forced vibration frequency for inhomogeneous shallow spherical and hypar shells consisting of IH_2 and IH_4 profiles are very close to those in the homogenous shells.

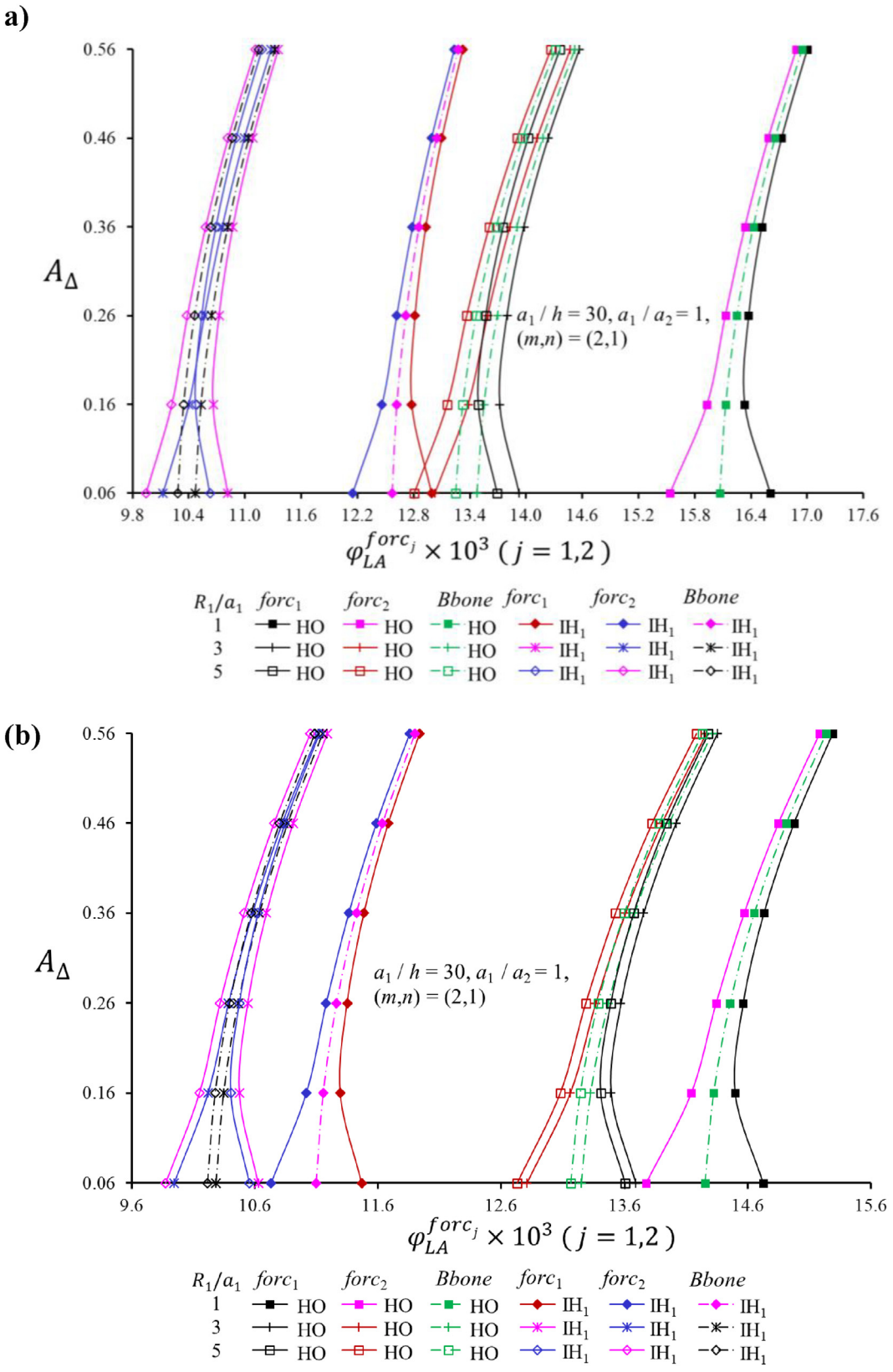

Fig. 4. Distribution of large amplitude forced vibration frequency of (a) inhomogenous spherical and (b) hypar shells depending on A_Δ for different R_1/a_1

Table 5
Variation of large amplitude forced vibration frequency of in homogenous spherical and hypar shells according to A_Δ for different R_1/a_1.

$\varphi_{LA}^{forc_j} \times 10^3$ $(j=1,2)$

		Hypar shells $(\eta_1,\eta_2)=(0,0)$ or HO			$(\eta_1,\eta_2)=(-1,0)$ or IH_1			Spherical shells $(\eta_1,\eta_2)=(0,0)$ or HO			$(\eta_1,\eta_2)=(-1,0)$ or IH_1		
R_1/a_1	A_Δ	$forc_1$	$forc_2$	*Bbone*	$forc_1$	$forc_2$	*Bbone*	$forc_1$	$forc_2$	*Bbone*	$forc_1$	$forc_2$	*Bbone*
1	0.06	14.726	13.777	14.251	11.467	10.728	11.098	16.604	15.534	16.069	12.989	12.151	12.570
	0.16	14.499	14.143	14.321	11.293	11.016	11.155	16.332	15.930	16.131	12.777	12.463	12.620
	0.26	14.564	14.345	14.455	11.348	11.178	11.263	16.373	16.126	16.250	12.812	12.619	12.716
	0.36	14.731	14.573	14.652	11.485	11.362	11.423	16.514	16.335	16.424	12.927	12.787	12.857
	0.46	14.975	14.851	14.913	11.683	11.587	11.635	16.725	16.586	16.656	13.099	12.989	13.044
	0.56	15.288	15.186	15.237	11.938	11.858	11.898	17.001	16.886	16.943	13.321	13.231	13.276
3	0.06	13.690	12.808	13.249	10.626	9.941	10.283	13.927	13.029	13.478	10.818	10.121	10.470
	0.16	13.490	13.159	13.324	10.473	10.216	10.344	13.721	13.384	13.552	10.661	10.399	10.530
	0.26	13.570	13.366	13.468	10.540	10.382	10.461	13.797	13.590	13.694	10.725	10.564	10.645
	0.36	13.754	13.607	13.680	10.691	10.577	10.634	13.977	13.827	13.902	10.873	10.756	10.814
	0.46	14.018	13.903	13.961	10.907	10.818	10.863	14.236	14.119	14.178	11.084	10.993	11.039
	0.56	14.357	14.262	14.310	11.183	11.110	11.147	14.569	14.473	14.521	11.355	11.281	11.318
5	0.06	13.604	12.727	13.166	10.555	9.875	10.215	13.690	12.808	13.249	10.626	9.941	10.283
	0.16	13.406	13.077	13.241	10.404	10.149	10.277	13.490	13.159	13.324	10.473	10.216	10.344
	0.26	13.487	13.285	13.386	10.473	10.316	10.395	13.570	13.366	13.468	10.540	10.382	10.461
	0.36	13.673	13.526	13.599	10.625	10.512	10.569	13.754	13.607	13.680	10.691	10.577	10.634
	0.46	13.939	13.825	13.882	10.843	10.754	10.798	14.018	13.903	13.961	10.907	10.818	10.863
	0.56	14.280	14.186	14.233	11.121	11.048	11.085	14.357	14.262	14.310	11.183	11.110	11.147

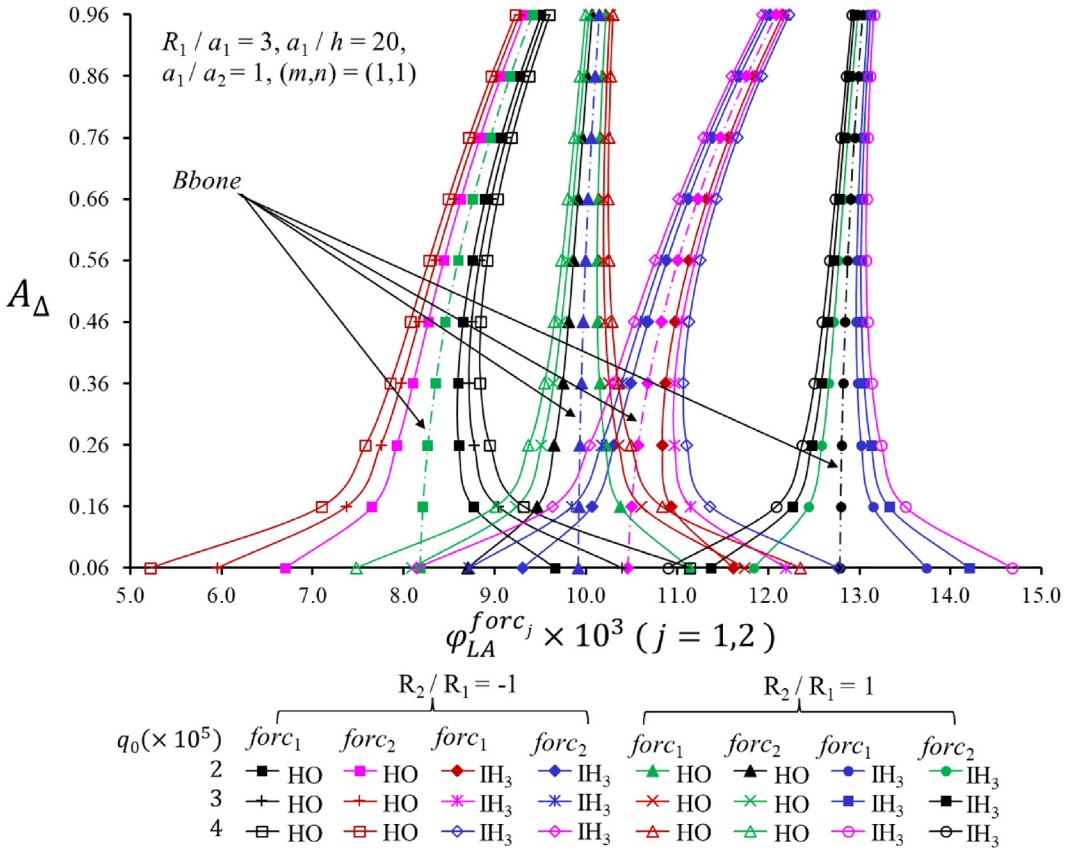

Fig. 5. Distributions of large amplitude forced vibration frequency of homogenous and inhomogenous-spherical and hypar shells depending on A_Δ for different excitation amplitude, q_0.

e) The influence of inhomogeneity profiles on the large amplitude forced vibration frequency values of inhomogeneous shallow spherical and hypar shells increases for the IH_1 profile, whereas decreases for IH_3 profile.

f) Due to the increase of a_1/h, the values of large amplitude forced vibration frequency for inhomogeneous shallow spherical and hypar shells decrease for all inhomogenety profiles except the IH_3 profile.

Table 6
Variations of large amplitude forced vibration frequency of homogenous and inhomogenous spherical and hypar shells according to A_Δ withdifferent q_0.

$\varphi_{LA}^{forc_j} \times 10^3$ $(j=1,2)$

		Hypar shells $(\eta_1,\eta_2)=(0,0)$ or HO			$(\eta_1,\eta_2)=(1,0)$ or IH_3			Spherical shells $(\eta_1,\eta_2)=(0,0)$ or HO			$(\eta_1,\eta_2)=(1,0)$ or IH_3		
q_0	A_Δ	$forc_1$	$forc_2$	$Bbone$	$forc_1$	$forc_2$	$Bbone$	$forc_1$	$forc_2$	$Bbone$	$forc_1$	$forc_2$	$Bbone$
2×10^5	0.06	9.656	6.698	8.177	11.615	9.302	10.458	11.136	8.699	9.918	13.731	11.841	12.786
	0.16	8.761	7.652	8.207	10.931	10.063	10.497	10.380	9.466	9.923	13.147	12.438	12.792
	0.26	8.604	7.922	8.263	10.838	10.305	10.572	10.215	9.652	9.933	13.022	12.585	12.804
	0.36	8.593	8.100	8.347	10.874	10.489	10.681	10.152	9.746	9.949	12.978	12.663	12.820
	0.46	8.650	8.264	8.457	10.977	10.676	10.827	10.128	9.810	9.969	12.966	12.719	12.843
	0.56	8.752	8.435	8.594	11.131	10.883	11.007	10.125	9.864	9.994	12.972	12.769	12.871
	0.66	8.892	8.623	8.758	11.329	11.118	11.223	10.136	9.914	10.025	12.990	12.818	12.904
	0.76	9.066	8.832	8.949	11.566	11.384	11.475	10.156	9.964	10.060	13.017	12.868	12.943
	0.86	9.270	9.063	9.167	11.843	11.681	11.762	10.185	10.015	10.100	13.053	12.921	12.987
	0.96	9.504	9.319	9.411	12.157	12.012	12.084	10.221	10.069	10.145	13.096	12.977	13.037
3×10^5	0.06	10.395	5.959	8.177	12.193	8.724	10.458	11.746	8.089	9.918	14.204	11.368	12.786
	0.16	9.039	7.375	8.207	11.148	9.847	10.497	10.609	9.237	9.923	13.324	12.260	12.792
	0.26	8.775	7.751	8.263	10.972	10.171	10.572	10.355	9.512	9.933	13.131	12.476	12.804
	0.36	8.716	7.977	8.347	10.970	10.392	10.681	10.253	9.644	9.949	13.057	12.584	12.820
	0.46	8.746	8.167	8.457	11.053	10.600	10.827	10.208	9.731	9.969	13.028	12.658	12.843
	0.56	8.832	8.356	8.594	11.193	10.821	11.007	10.190	9.799	9.994	13.023	12.719	12.871
	0.66	8.960	8.556	8.758	11.381	11.066	11.223	10.191	9.859	10.025	13.033	12.775	12.904
	0.76	9.124	8.774	8.949	11.612	11.338	11.475	10.204	9.916	10.060	13.055	12.831	12.943
	0.86	9.321	9.012	9.167	11.883	11.641	11.762	10.228	9.973	10.100	13.086	12.888	12.987
	0.96	9.550	9.273	9.411	12.193	11.976	12.084	10.260	10.031	10.145	13.125	12.948	13.037
4×10^5	0.06	11.135	5.219	8.177	12.771	8.145	10.458	12.355	7.480	9.918	14.677	10.895	12.786
	0.16	9.316	7.098	8.207	11.364	9.630	10.497	10.837	9.009	9.923	13.501	12.083	12.792
	0.26	8.946	7.581	8.263	11.105	10.038	10.572	10.496	9.371	9.933	13.240	12.367	12.804
	0.36	8.839	7.854	8.347	11.067	10.296	10.681	10.355	9.543	9.949	13.136	12.505	12.820
	0.46	8.843	8.071	8.457	11.128	10.525	10.827	10.287	9.651	9.969	13.089	12.596	12.843
	0.56	8.911	8.277	8.594	11.255	10.759	11.007	10.256	9.733	9.994	13.073	12.668	12.871
	0.66	9.027	8.489	8.758	11.434	11.013	11.223	10.246	9.803	10.025	13.076	12.732	12.904
	0.76	9.182	8.715	8.949	11.658	11.292	11.475	10.252	9.868	10.060	13.092	12.793	12.943
	0.86	9.373	8.960	9.167	11.923	11.601	11.762	10.270	9.930	10.100	13.119	12.855	12.987
	0.96	9.596	9.226	9.411	12.229	11.940	12.084	10.298	9.993	10.145	13.155	12.918	13.037

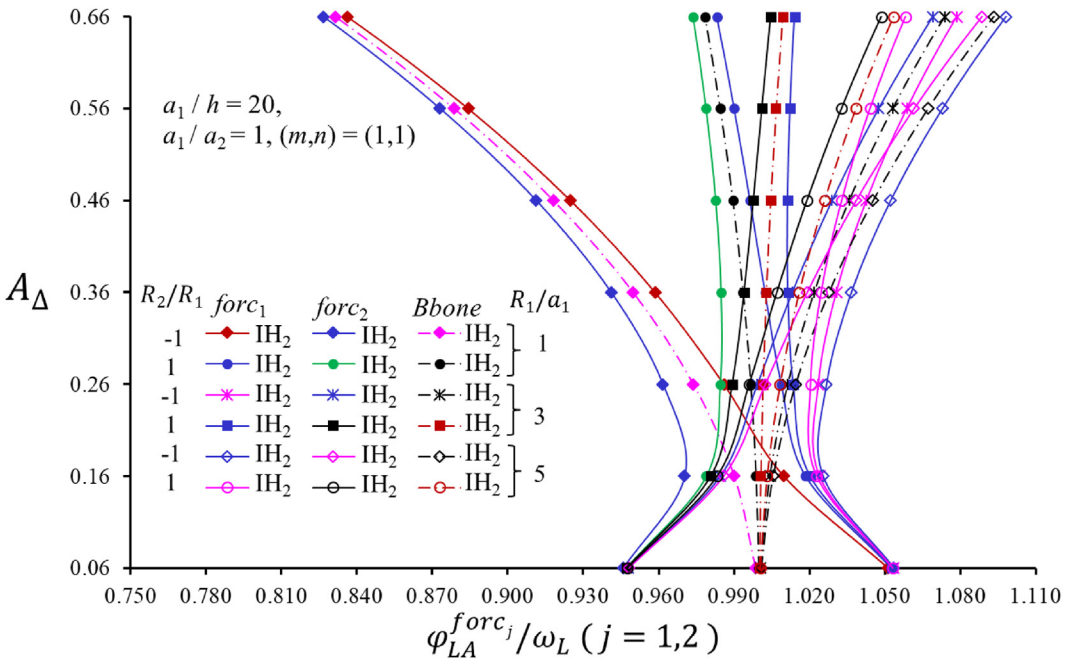

Fig. 6. Distributions of $\varphi_{LA}^{forc_j}/\omega_L$ $(j=1,2)$ of in homogenous spherical and hypar shells depending on A_Δ for different R_1/a_1

Table 7
Variations of $\varphi_{LA}^{forc_j}/\omega_L\,(j=1,2)$ for inhomogenous orthotropic hypar and spherical shells according to A_Δ with different R_1/a_1 ratio.

$\varphi_{LA}^{forc_j}/\omega_L\,(j=1,2)$							
		Hypar shells $(\eta_1,\eta_2)=(-1,-1)$ or IH_2			Spherical shells		
R_1/a_1	A_Δ	$forc_1$	$forc_2$	$Bbone$	$forc_1$	$forc_2$	$Bbone$
1	0.06	1.051	0.946	0.999	1.053	0.947	1.000
	0.16	1.010	0.970	0.990	1.019	0.979	0.999
	0.26	0.986	0.962	0.974	1.009	0.984	0.997
	0.36	0.959	0.941	0.950	1.002	0.985	0.994
	0.46	0.925	0.911	0.918	0.996	0.983	0.990
	0.56	0.884	0.873	0.879	0.990	0.979	0.984
	0.66	0.836	0.827	0.831	0.983	0.974	0.978
3	0.06	1.053	0.948	1.001	1.053	0.947	1.000
	0.16	1.024	0.985	1.004	1.020	0.981	1.001
	0.26	1.024	0.999	1.011	1.014	0.989	1.001
	0.36	1.031	1.013	1.022	1.012	0.994	1.003
	0.46	1.043	1.029	1.036	1.011	0.998	1.005
	0.56	1.059	1.047	1.053	1.012	1.001	1.007
	0.66	1.079	1.069	1.074	1.014	1.005	1.009
5	0.06	1.054	0.948	1.001	1.053	0.948	1.000
	0.16	1.025	0.986	1.005	1.023	0.983	1.003
	0.26	1.027	1.002	1.014	1.020	0.996	1.008
	0.36	1.037	1.019	1.028	1.025	1.007	1.016
	0.46	1.052	1.038	1.045	1.033	1.019	1.026
	0.56	1.073	1.061	1.067	1.044	1.033	1.038
	0.66	1.098	1.088	1.093	1.058	1.049	1.053

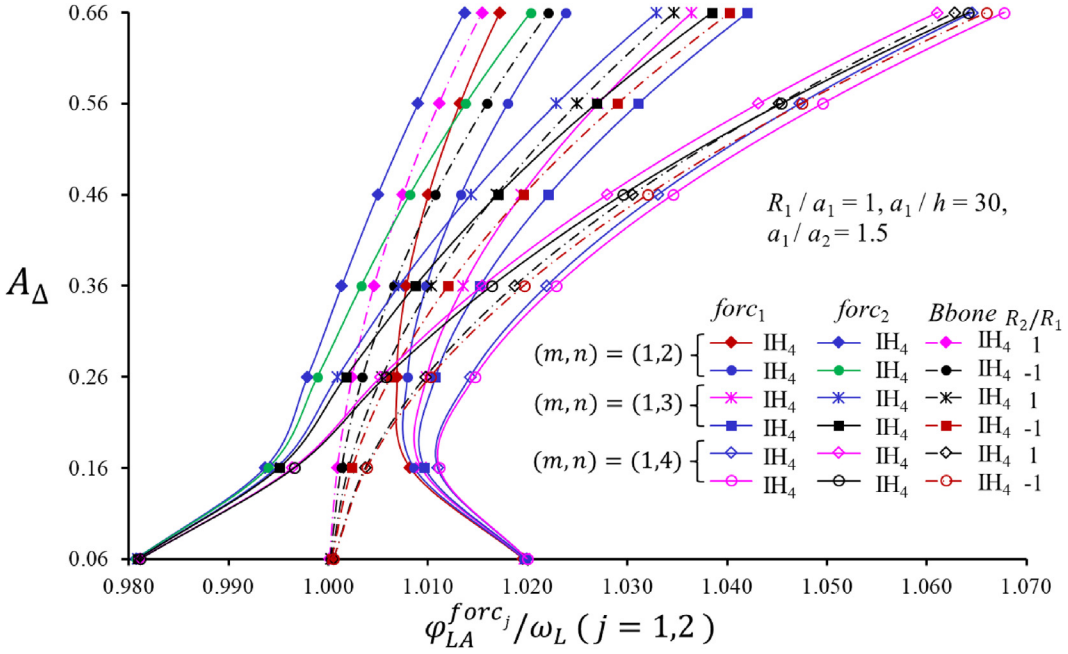

Fig. 7. Distributions of frequency ratio of in homogenous spherical and hypar shells depending on A_Δ for different modes $(1,n)$.

g) For a fixed nondimensional amplitude, the values of $\varphi_{LA}^{forc_1}$, $\varphi_{LA}^{forc_2}$ and ϖ_{LA}^{Bbone} decrease for both spherical and hypar shells, and this decrease rate turns out to be greater for the inhomogeneous orthotropic shallow spherical shell depending on the increase of R_1/a_1.
h) Depending on the increase of R_1/a_1, the change of the influence of the IH_1 profile is less than 1% for both shallow shells.
i) The difference of the inhomogeneity effect between the two shallow shells is increment due to the increase of excitation amplitude.
j) The values of large amplitude forced vibration frequency increase for both inhomogeneous shallow spherical and hypar shells depending on the increase of excitation amplitude for fixed nondimensional amplitude.
k) When the inhomogeneous shallow spherical and hypar shells are compared with each other, the highest ratio of nonlinear to linear frequencies occur in inhomogeneous hypar shells for $R_1/a_1>1$ and in inhomogeneous spherical shells for $R_1/a_1=1$.

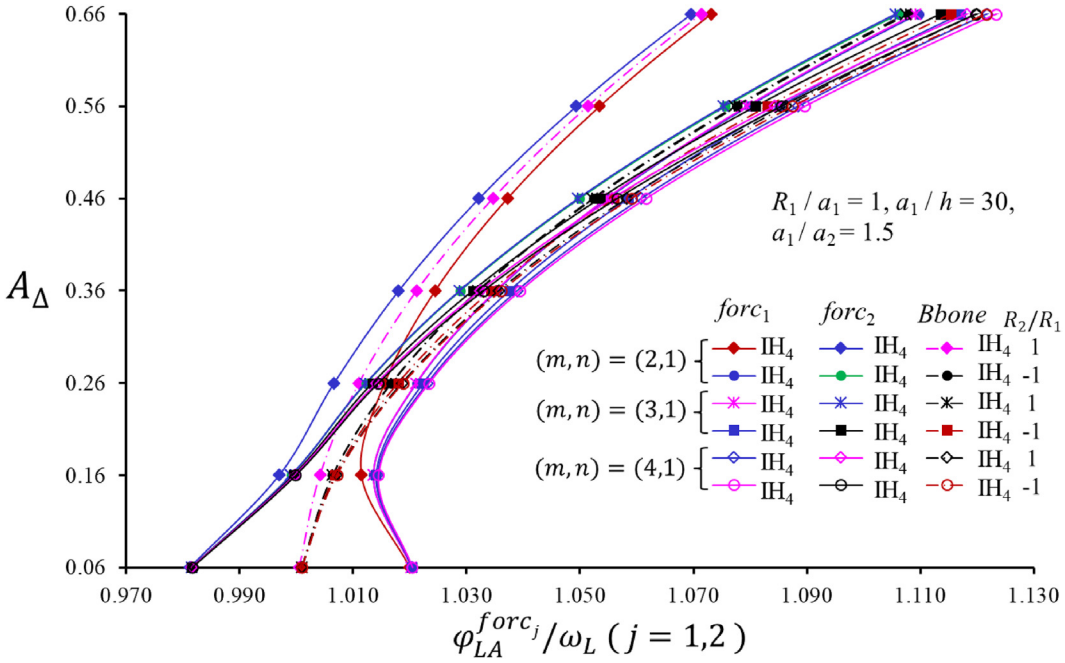

Fig. 8. Distributions of frequency ratio of in homogenous spherical and hypar shells depending on A_Δ for different modes $(m,1)$.

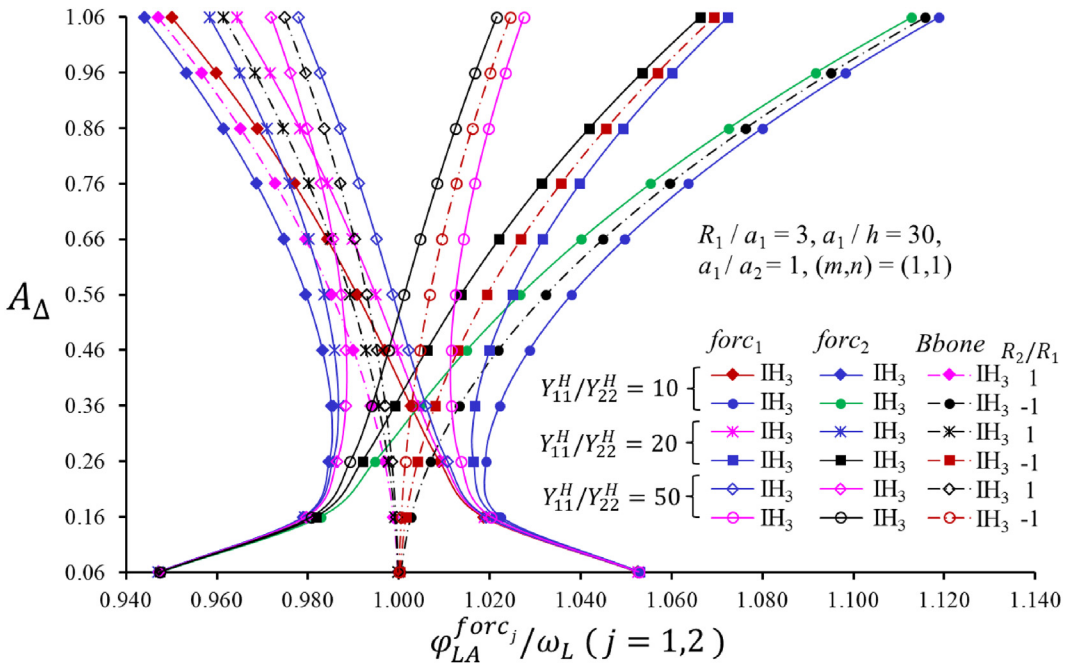

Fig. 9. Distrubitions of frequency ratio of in homogenous spherical and hypar shells depending on A_Δ for different Y_{11}^H/Y_{22}^H.

l) The ratios of $\varphi_{LA}^{forc_1}/\omega_L$, $\varphi_{LA}^{forc_2}/\omega_L$ and $\varpi_{LA}^{Bbone}/\omega_L$ increase, as the wave numbers (m,n) increase, and it should be emphasized that the frequency ratios are more pronounced for $n = 1$, as m increases.

m) The ratios $\varphi_{LA}^{forc_2}/\omega_L$ and $\varpi_{LA}^{Bbone}/\omega_L$ for both inhomogeneous shallow spherical and hypar shells increase, while the ratio $\varphi_{LA}^{forc_1}/\omega_L$ decreases and take its minimum value, then increases again depending on the increase of nondimensional amplitude.

n) The frequency ratio for inhomogeneous shallow spherical shells increases, while those decreases for inhomogeneous hypar shallow shells with the increasing of Y_{11}^H/Y_{22}^H.

Declaration of Competing Interest

The authors declare that they have no known competing financial interests or personal relationships that could have appeared to influence the work reported in this paper.

Table 8
Variations of frequency ratio of inhomogenous spherical and hypar shells according to A_Δ for different Y_{11}^H/Y_{22}^H.

$\varphi_{LA}^{forc_j}/\omega_L\ (j=1,2)$							
		Hypar shells $(\eta_1,\eta_2)=(1,0)$ or IH_3			Spherical shells		
Y_{11}^H/Y_{22}^H	A_Δ	$forc_1$	$forc_2$	$Bbone$	$forc_2$	$forc_1$	$Bbone$
10	0.06	1.053	0.947	1.000	1.053	0.948	1.000
	0.16	1.019	0.979	0.999	1.022	0.983	1.003
	0.26	1.009	0.985	0.997	1.019	0.995	1.007
	0.36	1.003	0.985	0.994	1.022	1.005	1.013
	0.46	0.997	0.983	0.990	1.029	1.015	1.022
	0.56	0.991	0.980	0.985	1.038	1.027	1.032
	0.66	0.984	0.975	0.979	1.050	1.040	1.045
	0.76	0.977	0.969	0.973	1.064	1.055	1.060
	0.86	0.969	0.961	0.965	1.080	1.073	1.076
	0.96	0.960	0.953	0.957	1.098	1.092	1.095
	1.06	0.950	0.944	0.947	1.119	1.113	1.116
20	0.06	1.053	0.947	1.000	1.053	0.947	1.000
	0.16	1.019	0.979	0.999	1.021	0.982	1.002
	0.26	1.010	0.986	0.998	1.016	0.992	1.004
	0.36	1.004	0.987	0.996	1.017	0.999	1.008
	0.46	1.000	0.986	0.993	1.020	1.006	1.013
	0.56	0.995	0.984	0.989	1.025	1.014	1.019
	0.66	0.990	0.980	0.985	1.032	1.022	1.027
	0.76	0.984	0.976	0.980	1.040	1.031	1.036
	0.86	0.978	0.971	0.975	1.049	1.042	1.046
	0.96	0.972	0.965	0.968	1.060	1.054	1.057
	1.06	0.964	0.958	0.961	1.072	1.066	1.069
50	0.06	1.053	0.947	1.000	1.053	0.947	1.000
	0.16	1.019	0.980	0.999	1.020	0.981	1.001
	0.26	1.011	0.986	0.998	1.014	0.989	1.001
	0.36	1.006	0.988	0.997	1.012	0.994	1.003
	0.46	1.002	0.988	0.995	1.011	0.998	1.005
	0.56	0.999	0.987	0.993	1.012	1.001	1.007
	0.66	0.995	0.985	0.990	1.014	1.005	1.009
	0.76	0.991	0.983	0.987	1.017	1.008	1.013
	0.86	0.987	0.980	0.983	1.020	1.012	1.016
	0.96	0.983	0.976	0.979	1.023	1.017	1.020
	1.06	0.978	0.972	0.975	1.027	1.021	1.024

Appendix A

The symbols contained in the Eqs. (6) and (7) are defined as follows:

$$\begin{gathered} C_{11}=A_{111}B_{11}+A_{121}B_{21},\ C_{12}=A_{111}B_{12}+A_{121}b_{11},\ C_{13}=A_{111}B_{13}+A_{121}B_{23}+A_{112},\\ C_{14}=A_{111}B_{14}+A_{121}B_{24}+A_{122},\ C_{21}=A_{211}B_{11}+A_{221}B_{21},\ C_{22}=A_{211}B_{12}+A_{221}B_{22},\\ C_{23}=A_{211}B_{13}+A_{221}B_{23}+A_{212},\ C_{24}=A_{211}B_{14}+A_{221}B_{24}+A_{222},\\ C_{31}=A_{661}B_{35},\ C_{32}=A_{661}B_{32}+2A_{662} \end{gathered} \tag{A1}$$

in which

$$\begin{gathered} B_{11}=\tfrac{A_{220}}{\nabla},\ B_{12}=-\tfrac{A_{120}}{\nabla},\ B_{13}=\tfrac{A_{120}A_{211}-A_{111}A_{220}}{\nabla},\ B_{14}=\tfrac{A_{120}A_{221}-A_{121}A_{220}}{\nabla},\\ B_{21}=-\tfrac{A_{221}}{\nabla},\ B_{22}=\tfrac{A_{110}}{\nabla},\ B_{23}=\tfrac{A_{111}A_{210}-A_{211}A_{110}}{\nabla},\ B_{24}=\tfrac{A_{121}A_{210}-A_{221}A_{110}}{\nabla},B_{31}=\tfrac{1}{A_{660}},\\ B_{32}=-\tfrac{2A_{661}}{A_{660}},\ \nabla=A_{110}A_{220}-A_{120}A_{210},\ A_{11k}=\int_{-h/2}^{h/2}q_{11}^{\tilde{x}_3}x_3^k dx_3\ A_{12k}=\int_{-h/2}^{h/2}\nu_{21}q_{11}^{\tilde{x}_3}x_3^k dx_3,\\ A_{21k}=\int_{-h/2}^{h/2}\nu_{12}q_{22}^{\tilde{x}_3}x_3^k dx_3,\ A_{22k}=\int_{-h/2}^{h/2}q_{22}^{\tilde{x}_3}x_3^k dx_3,\ c_{66}^k=\int_{-h/2}^{h/2}q_{66}^{\tilde{x}_3}x_3^k dx_3,\ k=0,1,2. \end{gathered} \tag{A2}$$

References

[1] Volmir AS. The nonlinear dynamics of plates and shells. Moscow: Science Edition; 1972.
[2] Nayfeh AH, Mook DT. Nonlinear oscillations. New York: John Wiley; 1979.
[3] Eschenauer H, Olhoff N, Schnell W. In: Applied Structural Mechanics. Berlin, Heidelberg: Springer Berlin Heidelberg; 1997. p. 241–300. https://doi.org/10.1007/978-3-642-59205-8_14.
[4] Amabili M. Classical nonlinear theories of doubly curved shells. Nonlinear mechanics of shells and plates in composite, soft and biological materials. Cambridge: Cambridge University Press; 2018. p. 60–89.
[5] Pan E. Exact solution for functionally graded anisotropic elastic composite laminates. J Compos Mater 2003;37(21):1903–20.
[6] Sofiyev AH, Schnack E. The buckling of cross-ply laminated non-homogeneous orthotropic composite conical thin shells under a dynamic external pressure. Acta Mech 2003;162(1-4):29–40.
[7] Ootao Y, Tanigawa Y. Three-dimensional solution for transient thermal stresses of an orthotropic functionally graded rectangular plate. Compos Struct 2007;80(1):10–20.
[8] Awrejcewicz J, Krysko VA. Theory of non-homogeneous shells. Chaos in structural mechanics. Berlin: Springer 2008:15–40.
[9] Grigorenko YM, Grigorenko AY. Static and dynamic problems for anisotropic inhomogeneous shells with variable parameters and their numerical solution. Int Appl Mech 2013;49(2):123–93.
[10] Nezhadi A, Rahman RA, Ayob A, Fard KM. Free and forced vibrations of FGM conical shell under impulse loads. Res J Appl Sci Eng Technol 2012;4(20):4055–65.
[11] Rafiee M, Mohammadi M, Sobhani Aragh B, Yaghoobi H. Nonlinear free and forced thermo-electro-aero-elastic vibration and dynamic response of piezoelectric functionally graded laminated composite shells, Part I: Theory and analytical solutions. Compos Struct 2013;103:179–87.
[12] Du C, Li Y, Jin X. Nonlinear forced vibration of functionally graded cylindrical thin shells. Thin-walled Struct 2014;78:26–36.
[13] Awrejcewicz J, Kurpa L, Shmatko T. Analysis of geometrically nonlinear vibrations of functionally graded shells of a complex shape. Latin Am J Solid Struct 2017;14:1648–68.
[14] Sheng GG, Wang X. The non-linear vibrations of rotating functionally graded cylindrical shells. Nonlinear Dyn 2017;87(2):1095–109.
[15] Sheng GG, Wang X. Nonlinear vibrations of FG cylindrical shells subjected to parametric and external excitations. Compos Struct 2018;191:78–88.
[16] Awrejcewicz J, Kurpa L, Shmatko T. Linear and nonlinear free vibration analysis of laminated functionally graded shallow shells with complex plan form and different boundary conditions. Int J Non Linear Mech 2018;107:161–9.
[17] Amabili M. Composite, sandwich and functionally graded materials: Advanced nonlinear shell theories. Nonlinear mechanics of shells and plates in composite, soft and biological materials. Cambridge: Cambridge University Press; 2018. p. 90–123.
[18] Sobhy M, Zenkour AM. Vibration analysis of functionally graded graphene platelet-reinforced composite doubly-curved shallow shells on elastic foundations. Steel Compos Struct 2019;33(2):195–208.
[19] Karimiasl M, Ebrahimi F, Mahesh V. Nonlinear free and forced vibration analysis of multiscale composite doubly curved shell embedded in shape-memory alloy fiber under hygrothermal environment. J Vib Control 2019;25(13):1945–57.

[20] Zhu Bo, Xu Qi, Li M, Li Y. Nonlinear free and forced vibrations of porous functionally graded pipes conveying fluid and resting on nonlinear elastic foundation. Compos Struct 2020;252:112672. https://doi.org/10.1016/j.compstruct.2020.112672.
[21] Sofiyev AH, Turan F, Zerin Z. Large-amplitude vibration of functionally graded orthotropic double-curved shallow spherical and hyperbolic paraboloidal shells. Int J Press Vessels Pip 2020;188:104235. https://doi.org/10.1016/j.ijpvp.2020.104235.
[22] Thai H-T, Kim S-E. Levy-type solution for free vibration analysis of orthotropic plates based on two variable refined plate theory. Appl Math Model 2012;36(8):3870–82.
[23] Reddy JN. Mechanics of laminated composite plates and shells: theory and analysis. CRC Press; 2004.